Supplementary Information for:

Blending induced stack-ordering and performance improvement in a solution-processed *n*-type organic field-effect transistor

Zhongming Wei,[a,b] Hongxia Xi,[a,b] Huanli Dong,[a] Linjun Wang,[a] Wei Xu,*[a] Wenping Hu*[a] and Daoben Zhu*[a]

[a]Beijing National Laboratory for Molecular Sciences, Key Laboratory of Organic Solids, Institute of Chemistry, Chinese Academy of Sciences, Beijing 100190, and [b]Graduate University of the Chinese Academy of Sciences, Beijing 100039, P. R. China.

E-mail: wxu@iccas.ac.cn and zhudb@iccas.ac.cn

1. Optical, electrochemical and thermal properties of PTCDI-e.

The UV-vis absorption and FL emission spectra of PTCDI-e in $CHCl_3$ solution and thin film are shown in Figure S1. Compared with the peaks in the solution, the absorptions in thin film become broad with red-shift of 28, 36, 41 nm, respectively. The red shifts indicated the edge-to-face molecular aggregation (*i.e.* J-aggregation) in the solid state.

Figure S2 shows the cyclic voltammogram of PTCDI-e solution. Two reversible reduction waves were observed, but no oxidation wave could be observed. With the half-wave reduction potential $E_{1/2}$ = 1/2(-0.544-0.62) = -0.582 V and using the ferrocene/ferrocenium (Fc/Fc^+) as an internal standard, the LUMO level was determined by E_{LUMO}= -[4.8 – E_{FOC} + $E_{1/2}^{red}$] eV ≈ -[4.4 + $E_{1/2}^{red}$] eV = -3.82 eV. From the solution absorption edge (Figure S1a), the HOMO-LUMO gap was calculated at 1.89 eV. According to the LUMO level and the HOMO-LUMO gap, the HOMO level was calculated at -5.71 eV.

The thermal properties of PTCDI-e are shown in Figure S3. Thermogravimetric analysis (TGA) displayed that PTCDI-e had good thermal stability with a high decomposition temperature. Two

endothermal peaks in the differential thermal analysis (DTA) indicated the appearance of liquid crystalline phase and the first one corresponding to the phase transition from solid to a highly ordered mesophase.

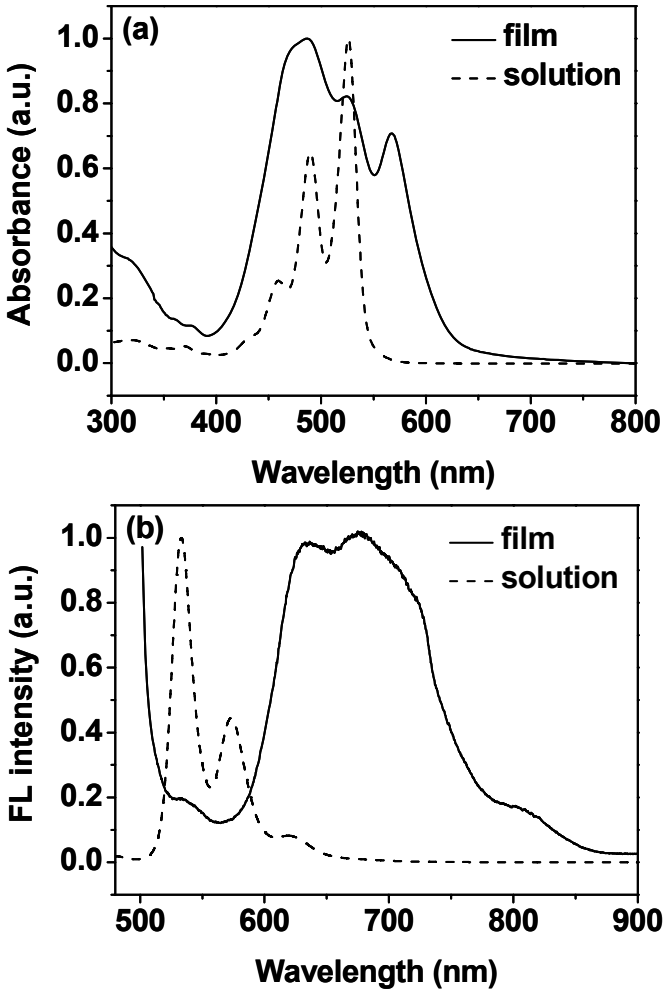

Figure S1. (a) UV-vis absorption and (b) FL emission spectra of PTCDI-e in $CHCl_3$ solution and thin film.

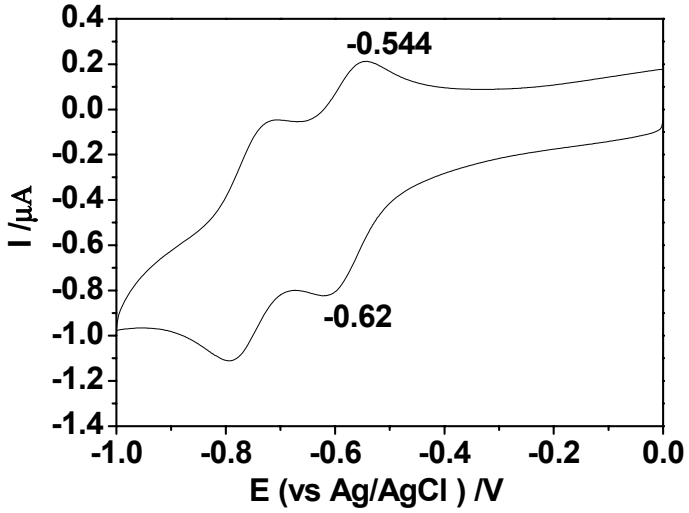

Figure S2. Cyclic voltammogram for PTCDI-e (0.1 mM compound and 0.1 M Bu_4NPF_4 in CH_2Cl_2, Ag/AgCl as reference electrode and ferrocene as internal standard, scan rate 100 mV/s).

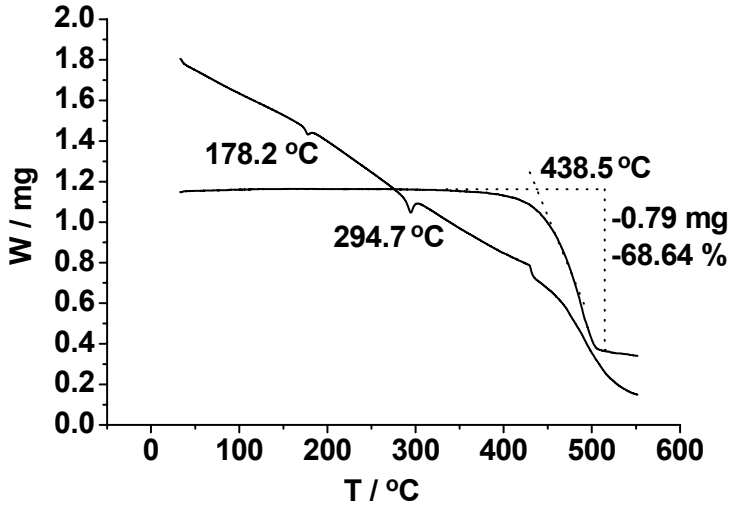

Figure S3. TGA and DTA plots of PTCDI-e with a heating rate of 10 ^{o}C /min under N_2.

2. Vacuum-Deposited OFETs.

PTCDI-e was vacuum deposited both on the bare and octadecyltrichlorosilane (OTS) treated Si/SiO_2 substrates with different substrate temperature (T_S) in the top-contact configuration to fabricate OFET devices. Thin films (50 nm thick) were vacuum deposited at 0.4 Å/s. The deposition rate and film

thickness were monitored by ULVAC CRTM-6000. All the devices were measured in vacuum. The performance data including electron field-effect mobility (μ), on/off current ration (I_{on}/I_{off}), and threshold voltage (V_T) are summarized in Table S1. The best performance (μ = 0.279 $cm^2 V^{-1} s^{-1}$, I_{on}/I_{off} = 1.1×10^6, V_T = 2.6 V) was obtained from the devices fabricated on the bare Si/SiO_2 substrate at T_S = 150 ^oC. Figure S4 shows the transfer and output curves of a typical device.

The electron mobility was increased with the increasing of the substrate temperature both for the two different substrates. This can be explained by the crystallization and grain size. Figure S5 and Figure S6 show the X-ray diffraction (XRD) patterns and atomic force microscopy (AFM) images of the films. The increasing intensities resulted from the increase of the substrate temperature indicated the improvements of the crystallinity of films and ordering between molecular chains. High crystallinity and order caused strong intermolecular π-π stacking, which benefited the transport of charge carriers. Also, the size of the crystal grains stacking by molecular terraces increased with the increase of the substrate temperature. Larger grains resulted in fewer defects between the grain boundaries and higher mobility. Height of a terrace in the grains was calculate at 3.20 ± 0.1 nm by AFM, which is refer to the molecular length and corresponding to the (001) reflection at 3.20 nm (2θ = 2.76°) in Figure 4a.

Table S1. OFET performances of the vacuum-deposited devices.

substrate	T_S (^oC)	μ ($cm^2 V^{-1} s^{-1}$)	I_{on}/I_{off}	V_T (V)
Bare	28 (RT)	0.052	1.0×10^8	10.5
	60	0.115	1.4×10^8	12.6
	100	0.117	8.0×10^7	12.0
	150	0.279	1.1×10^6	2.6
Ots	28 (RT)	0.071	1.3×10^8	13.7
	60	0.107	7.0×10^7	17.6
	100	0.163	3.0×10^8	17.5
	150	0.165	1.1×10^6	4.7

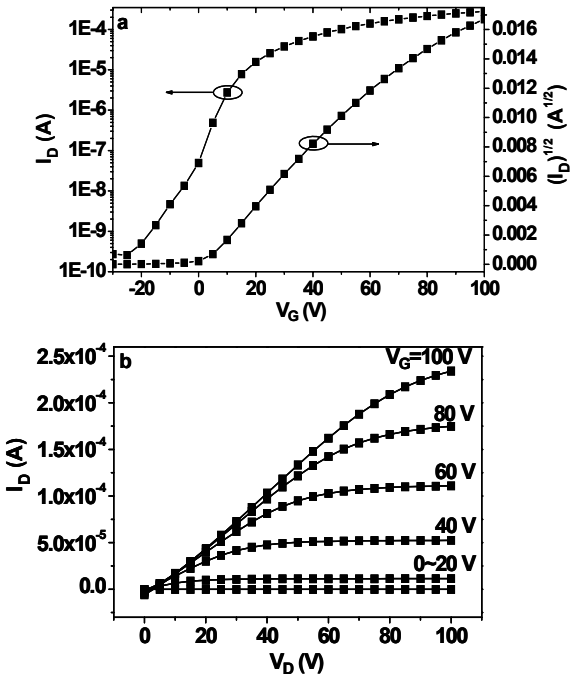

Figure S4. (a) Transfer (V_D = 100 V) and (b) output curves of the OFET fabricated on the bare Si/SiO_2 substrate at T_S = 150 ^oC.

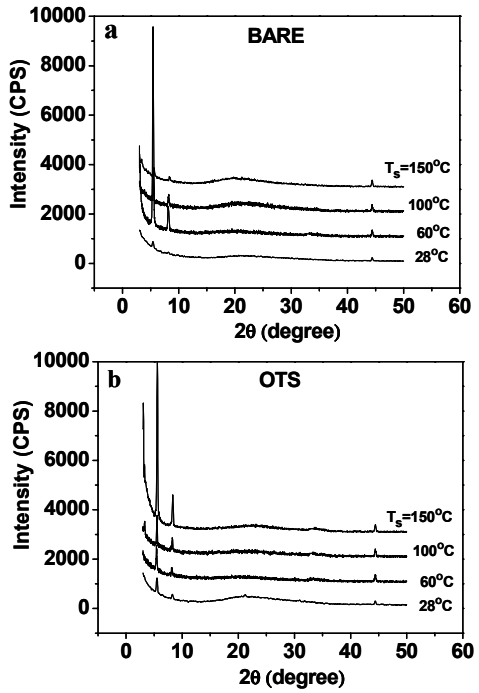

Figure S5. XRD patterns of the films deposited at different temperature: (a) bare Si/SiO_2 substrate and (b) OTS treated Si/SiO_2 substrate.

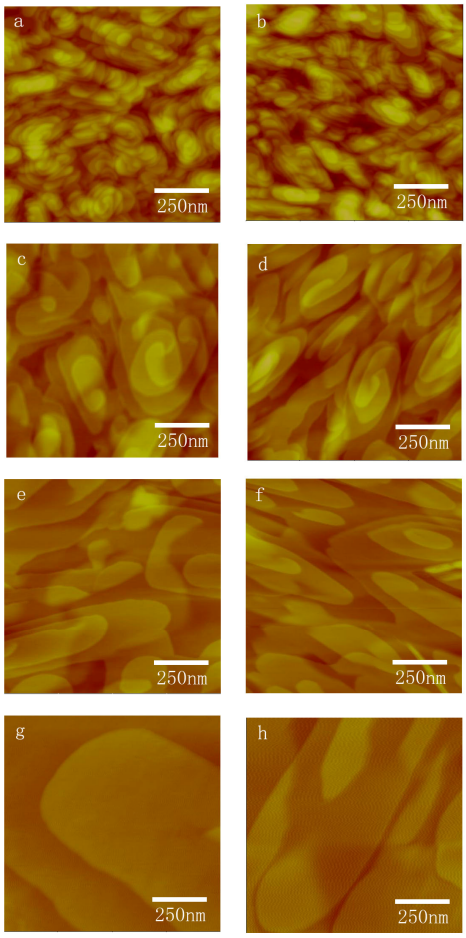

Figure S6. AFM images of the films deposited on: bare Si/SiO_2 substrate: (a) T_S = 28 °C, (c) T_S = 60 °C, (e) T_S = 100 °C, (g) T_S = 150 °C; OTS treated Si/SiO_2 substrate: (b) T_S = 28 °C, (d) T_S = 60 °C, (f) T_S = 100 °C, (h) T_S = 150 °C. (height scale 50 nm)

3. Solution-Processed films.

Table S2. Typical I_{off} and I_{on} of the PTCDI-e solution-processed OFETs.

blend materials	blending ratio (mol %)	I_{off} (A)	I_{on} (A)
TMTSF[a]	0	9.67×10^{-11}	4.11×10^{-6}
	9.05	5.43×10^{-11}	1.38×10^{-5}
	16.59	7.11×10^{-11}	1.87×10^{-5}
	28.46	1.46×10^{-9}	1.29×10^{-4}
	44.31	9.78×10^{-11}	2.59×10^{-5}
	54.41	3.76×10^{-11}	1.27×10^{-5}
TTF[b]	0	3.35×10^{-10}	1.89×10^{-6}
	17.86	4.51×10^{-10}	3.07×10^{-6}
	30.31	4.49×10^{-10}	3.67×10^{-6}
	46.52	5.41×10^{-10}	8.97×10^{-6}
	63.50	1.03×10^{-9}	1.38×10^{-5}
	72.30	2.78×10^{-10}	3.80×10^{-5}
	77.68	2.61×10^{-10}	5.15×10^{-5}
	81.31	1.93×10^{-10}	1.65×10^{-5}
TCNQ[b]	0	3.35×10^{-10}	1.89×10^{-6}
	17.86	2.28×10^{-10}	1.30×10^{-6}
	30.31	5.07×10^{-10}	5.96×10^{-7}
	46.52	2.11×10^{-10}	7.19×10^{-7}
	63.50	2.82×10^{-10}	6.44×10^{-7}

[a]Annealed at 150 ^{o}C after deposition. [b]Annealed at 50 ^{o}C after deposition.

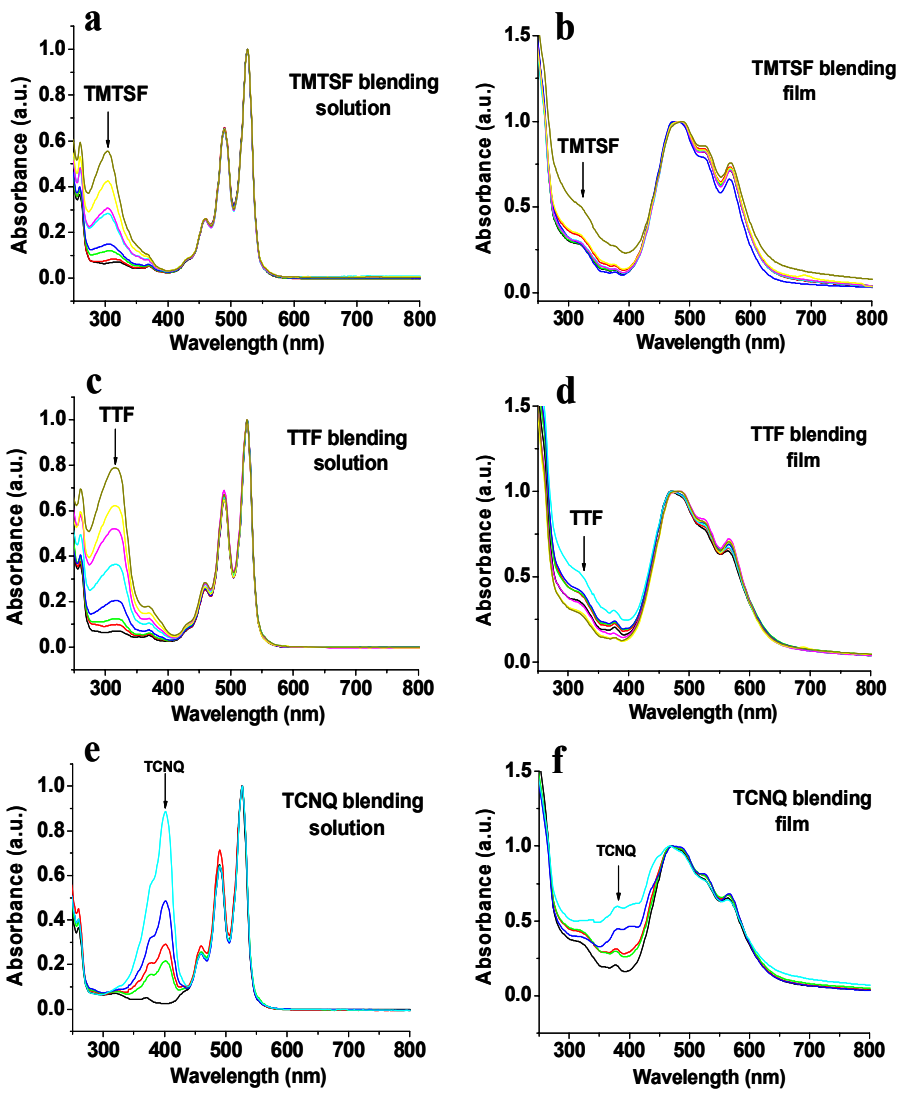

Figure S7. UV-vis absorption spectra of the blended PTCDI-e solutions and solid films.

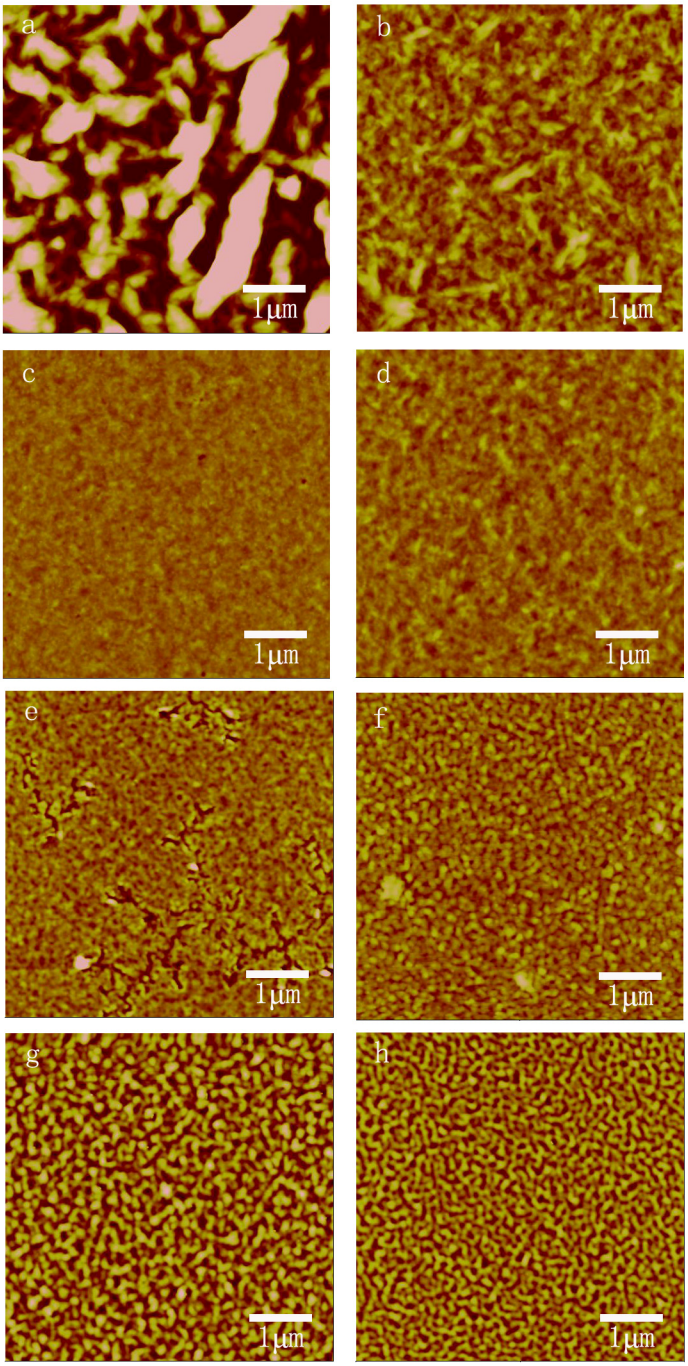

Figure S8. AFM images of the solution-processed PTCDI-e films blended with TTF at different ratios: (a) 0, (b) 17.86, (c) 30.31, (d) 46.52, (e) 63.50, (f) 72.30, (g) 77.68, (h) 81.31 mol %. (height scale 50 nm)

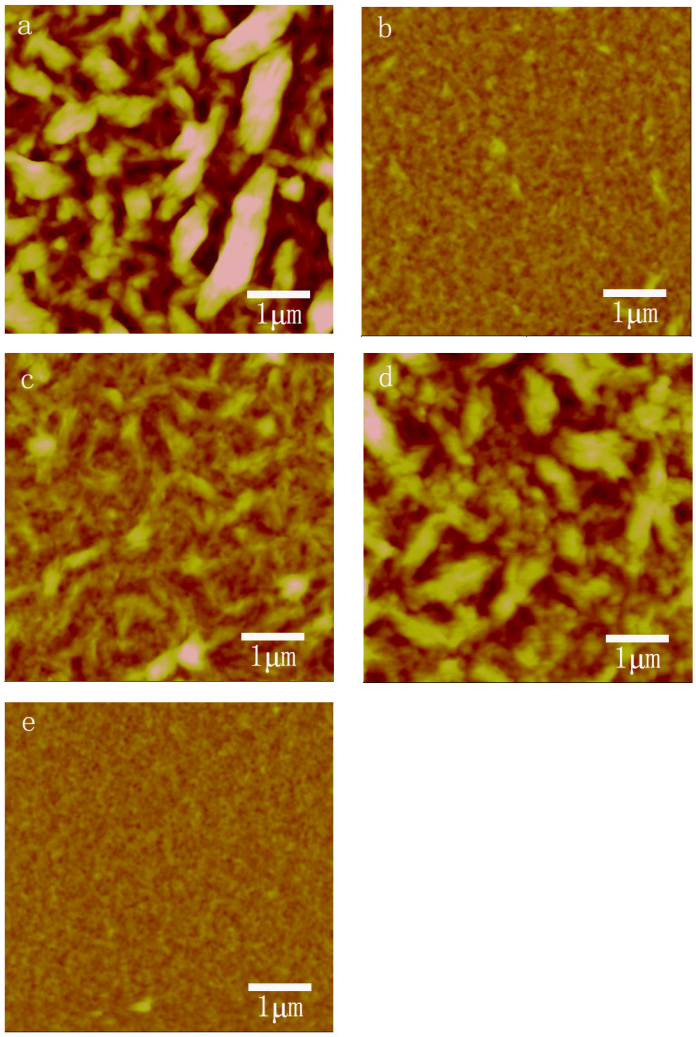

Figure S9. AFM images of the solution-processed PTCDI-e films blended with TCNQ at different ratios: (a) 0, (b) 17.86, (c) 30.31, (d) 46.52, (e) 63.50 mol %. (height scale 50 nm)